Spectral properties of strongly correlated multi-impurity models in the Kondo insulator regime: Emergent coherence, metallic surface states, and quantum phase transitions

Fabian Eickhoff and Frithjof B. Anders
Fakultät Physik, Technische Universität Dortmund, 44221 Dortmund, Germany

(Received 27 July 2021; revised 15 September 2021; accepted 16 September 2021; published 4 October 2021)

We investigate the real-space spectral properties of strongly correlated multi-impurity arrays in the Kondo insulator regime. Employing a recently developed mapping onto an effective correlated cluster problem makes the problem accessible to the numerical renormalization group. The evolution of the spectrum as a function of cluster size and cluster site is studied. We applied the extended Lieb-Mattis theorem to predict whether the spectral function must vanish at the Fermi energy developing a true pseudogap or whether the spectral function remains finite at $\omega = 0$. Our numerical renormalization group spectra confirm the predictions of the theorem and shows a metallic behavior at the surface of a cluster prevailing in arbitrary spatial dimensions. We present a conventional minimal extension of a particle-hole symmetric Anderson lattice model at $U = 0$ that leads to a gapped bulk band but a surface band with mainly f-orbital character for weak and moderate hybridization strength. The change in the site-dependent spectra upon introducing a Kondo hole in the center of the cluster is presented as a function of the hole-orbital energy. In particular, the spectral signatures across the Kosterlitz-Thouless-type quantum phase transition from a singlet to a local moment fixed point are discussed.

DOI: 10.1103/PhysRevB.104.165105

I. INTRODUCTION

Multi-impurity Anderson models (MIAMs) [1–4] and its Kondo model counterparts have a long history in strongly correlated materials. The basic properties of heavy Fermions (HFs) [3,5] can be understood in terms of a hybridized band picture responsible for the heavy Fermi liquid (FL) [6] emerging from the coupling between the light itinerant conduction electrons and strongly localized and correlated f orbitals. The discovery of superconductivity [7] and competing magnetic order [3,8] in such materials has generated a large interest in this material class over the last 40 years.

One special incarnation of such a system is Kondo insulators, where a correlation-induced gap opens up [9–11]: The resistivity increases below a characteristic temperature scale of the lattice, and the material crosses over from a metal to an insulator with a very small band gap when lowering the temperature. Triggered by the advent of topological insulators, such Kondo insulators have again drawn a lot of experimental and theoretical interest. Particular there is an active debate on whether SmB_6 can be classified as a topological Kondo insulator [12,13] or a trivial surface conductor [11]. Local density approximations [14] in combination with Gutzwiller methods [15] strongly indicate a topological nature of SmB_6, although the Kondo physics in such materials cannot be addressed by those approaches. In topological insulators [16], the protection of the Chern number enforces metallic edge states. This single-particle band properties, induced by spin-orbit coupling, inspired a lot of theoretical activity [17–20] to address the experimental findings of a metallic surface state [11–13] in Kondo insulators by converting the conventional Kondo lattice or periodic Anderson model (PAM) with a spin-orbit coupling term into a topological Kondo insulator in which a metallic surface emerges naturally from topological constrains.

In this paper, we present site-dependent spectral functions of a MIAM comprising a finite number of correlated orbitals embedded in a bipartite lattice of uncorrelated orbitals. Our conventional starting point [6,21] does not take into account the spin-orbit coupling in the Ce $4f$ shell considered by Dzero *et al.* [17] and, therefore, cannot address a topological Kondo insulator.

Raczkowski and Assaad reported a metallic surface layer in a finite-size Kondo nanocluster studied with a finite temperature auxiliary-field quantum Monte Carlo (QMC) algorithm. The authors realized that this spectral feature is unrelated to topological properties and interpreted their results [22] as decoupling of the metallic surface from the bulk properties.

We argue that the emerging metallic surface is a consequence of the extended Lieb-Mattis theorem [23,24] that can be applied to an arbitrarily large finite-size correlated cluster of a very simple MIAM. On the contrary, in a conventional pristine Kondo lattice model or periodic Anderson model, the surface remains insulating at half filling. In this paper, we present a simple argument based on this theorem—how to predict whether a local spectral function must vanish at $\omega = 0$ or a finite density of states is found. We successfully employ this argument to understand the elementary real-space spectral properties of a MIAM cluster obtained with Wilson's numerical renormalization group (NRG) approach [25,26]. In particular, the argument rigorously predicts a nonvanishing spectral density in the f-orbital spectra on the surface of a Kondo insulator cluster in agreement with auxiliary-field QMC data [22] and our NRG spectra.

To reconcile the insulating surface of a pristine Kondo insulator model with the findings of a metallic surface state in a finite-size but arbitrarily large Kondo insulator cluster embedded in a metallic host, we address the question, What is the minimum extension of a Kondo insulator to generate a metallic surface without invoking the well-discussed topological arguments? It turns out to be sufficient to include only one additional layer of noninteracting orbitals to generate a metallic surface band. We present a mean-field tight-binding calculation of a $2d$ Kondo lattice stripe to demonstrate the emerging of exactly two spin-degenerate metallic surface bands involving only the edge orbitals. While for weak hybridization, the surface band mainly has an f character close to Fermi energy, the uncorrelated edge orbital starts to dominate once the hybridization strength exceeds the single-particle hopping matrix element. This finding opens the door for speculations whether the metallic properties of the surface band in Kondo insulators might be related to ruggedness of the surface edge.

We present the evolution of the spectral function in a finite-size $1d$ MIAM to study the crossover from single-impurity surface physics to correlated bulk properties. We find that the gap size at the cluster center agrees excellently with those obtained from a dynamical mean field (DMFT) calculation [27,28] for an infinitely large Kondo lattice model. From the recently developed mapping of the problem onto an effective cluster [4], it becomes apparent that a single impurity Kondo model is insufficient to understand the screening of the local moments (LMs), as already suspected by Nozières [29]. The spin moment screening mechanism in the Kondo lattice model can be better understood in terms of self-screening [30] after mapping the model onto an emerging Hubbard model that is also responsible for the band formation.

We extend our study to the site-dependent spectral properties of the Kondo-hole problem. In particular, we track the spectral evolution close to the Kosterlitz-Thouless-type quantum phase transition (QPT) from a strong-coupling fixed point (FP) to a LM FP describing the LM formation by a charge-neutral substitution of a correlated orbital in a Kondo insulator [24,31]. The spectral properties explicitly reveal the occurrence of a second Kondo temperature well below the lattice coherence temperature responsible for a sharp Kondo resonance that develops in the gap of the Kondo insulator.

The paper is organized as follows: Section II is devoted to defining the model under consideration and a very brief review of our recently developed mapping onto an effective model [4], which we employ to calculate the spectral functions using the NRG. In particular, the matrix generalization of the equation of motion approach by Bulla *et al.* [32] is presented. We present our results in Sec. III. We start with the spectral evolution as a function of the cluster size in Sec. III A. Section III B is devoted to the application of the extended Lieb-Mattis theorem [24] to predict whether the spectral function must vanish at $\omega = 0$ or not. We demonstrate that our NRG calculations are fully in line with the prediction of this theorem, providing a better understanding of the observed zero frequency features at certain lattice sites. The site-dependent evolution of the spectral functions is presented in Sec. III C for the largest cluster we can access within the NRG. We augment our findings with a tight-binding $U = 0$ calculation for an infinitely large $2d$ stripe model with periodic boundary conditions in one dimension to demonstrate the emergence of a metallic surface band in Sec. III C 2. The last part of the Results section, Sec. III D, is devoted to the evolution of the spectral properties in the vicinity of a Kondo hole. In particular, we trace the breakdown of the Kondo screening of the emerging LM close to the QPT. We close the paper with a short conclusion.

II. MULTI-IMPURITY MODELS AND KONDO HOLES

A. Hamiltonian

The MIAM [4] comprises two subsystems: the uncorrelated conduction electrons and the localized correlated f electrons. The uncorrelated condition electrons are modeled by a tight-binding model,

$$H_{\text{host}} = \sum_{\substack{i,j,\sigma \\ i \neq j}} \left(-t_{ij} c^\dagger_{i,\sigma} c_{j,\sigma} + \epsilon^c_i c^\dagger_{i,\sigma} c_{i,\sigma}\right), \tag{1}$$

where t_{ij}, ϵ^c_i denote the transfer parameter and single-particle energy, and i, j labels the lattice sites of the underlying lattice. We assume translational invariance of this subsystem so this Hamiltonian is diagonal in k space and the single-particle dispersion is denoted by $\epsilon_{\vec{k}\sigma}$. In principle, a Zeemann energy can be included but we only consider the system in the absence of an external magnetic field.

The localized f electrons are described by the atomic part of a Hubbard Hamiltonian,

$$H_{\text{corr}} = \sum_{l,\sigma} \epsilon^f_l f^\dagger_{l,\sigma} f_{l,\sigma} + H_{\text{int}}, \tag{2}$$

$$H_{\text{int}} = \sum_{l} U_l f^\dagger_{l,\uparrow} f_{l,\uparrow} f^\dagger_{l,\downarrow} f_{l,\downarrow}, \tag{3}$$

on a subset of N_f lattice sites $l \in i$. $f^{(\dagger)}_l$ destroys (creates) an electron on impurity l, whose on-site energy is labeled by ϵ^f_l, and U accounts for the on-site Coulomb repulsion. A local single particle hopping term,

$$H_{\text{hyb}} = \sum_{l,\sigma} V_l c^\dagger_{l,\sigma} f_{l,\sigma} + \text{H.c.}, \tag{4}$$

facilitates the hopping of an electron between the localized f orbital and the corresponding Wannier orbital at the same lattice site. V_l denotes the local hybridization of the impurity at lattice site l with the corresponding local lattice orbital, such that the total Hamiltonian is given by

$$H = H_{\text{host}} + H_{\text{corr}} + H_{\text{hyb}}. \tag{5}$$

For l running over all lattice sites of the host, we obtain the periodic Anderson model. If $N_f = 1$, we recover the well-understood single impurity model. By setting individual values for ϵ^f_l, U_l at specific lattice sites, we include the modeling of Kondo holes into our rather general description [24]. Such a setup is schematically depicted in Fig. 1 for $N_f = 7$. We can also set $\epsilon^f_l = \epsilon^f_h$ at the location $h \in l$ of the Kondo hole and send ϵ^f_h to very large value to completely deplete that particular orbital.

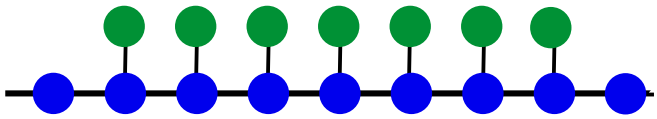

FIG. 1. Sketch of the geometric setup: An array of $N_f = 7$ correlated f orbitals (green) are locally coupled to a $1d$ tight binding chain (blue) with the number of conduction band orbitals, N_c, larger than N_f to define a band continuum.

B. Mapping of the MIAM and Green's functions

Here we briefly review the mapping of the MIAM onto an effective multiband model in the wide band limit which we developed recently [4] and already applied to the Kondo-hole problem [24]. In a translation invariant lattice, the Hamiltonian H_{host} becomes diagonal in $\vec{k}$ space:

$$H_{\text{host}} = \sum_{\vec{k}\sigma} \epsilon_{\vec{k}\sigma} c^\dagger_{\vec{k}\sigma} c_{\vec{k}\sigma}. \tag{6}$$

We define the coupling function matrix element $\Delta_{l,l'}(z)$ [4,33],

$$\Delta_{l,l',\sigma}(z) = V_l V_{l'}^* D^\sigma_{l,l'}(z), \tag{7}$$

where $D^\sigma_{l,l'}(z)$ denotes the unperturbed Green's function (GF) of the noninteracting host in real space:

$$D^\sigma_{l,l'}(z) = \frac{1}{N} \sum_{\vec{k}} \frac{1}{z - \epsilon_{\vec{k}\sigma}} e^{i\vec{k}(\vec{R}_l - \vec{R}_{l'})}. \tag{8}$$

Then, the exact real-space multi-impurity GF is a matrix of dimension $N_f \times N_f$ and takes the form

$$\boldsymbol{G}^f_\sigma(z) = [z - \boldsymbol{E}_\sigma - \boldsymbol{\Delta}_\sigma(z) - \boldsymbol{\Sigma}_\sigma(z)]^{-1}, \tag{9}$$

where the matrix $\boldsymbol{E}_\sigma$ contains the single-particle energies of the localized f orbitals and $\boldsymbol{\Sigma}(z)$ denotes the self-energy matrix. Using the exact equation of motion for the GFs, it is straightforward to show that

$$\boldsymbol{\Sigma}_\sigma(z) = \boldsymbol{F}_\sigma \left[\boldsymbol{G}^f_\sigma\right]^{-1}, \tag{10}$$

and the matrix elements of the correlation matrix $\boldsymbol{F}$ are defined as [32]

$$F_{l,l',\sigma}(z) = G_{B_{l\sigma}, f^\dagger_{l'\sigma}}(z), \tag{11}$$

where the composite operator $B_{l\sigma}$ is generated by the commutator:

$$B_{l\sigma} = [f_{l\sigma}, H_{\text{int}}] = U_l f_{l\sigma} f^\dagger_{l\bar{\sigma}} f_{l\bar{\sigma}}. \tag{12}$$

Note that the operator $B_{l\sigma}$ has the dimension energy and reads explicitly where $\bar{\sigma} = -\sigma$.

Since the host degrees of freedom are uncorrelated, the local host GF in the presence of the correlated orbitals obeys the exact relation,

$$G_{c_{i\sigma}, c^\dagger_{j\sigma}}(z) = D^\sigma_{i,j}(z) + \sum_{l_1,l_2} D^\sigma_{i,l_1}(z) V_{l_1} G^f_{l_1,l_2}(z) V^*_{l_2} D^\sigma_{l_2,j}(z), \tag{13}$$

which can be casted into a matrix multiplication. While $D^\sigma_{i,j}(z)$ describes the free propagation of a conduction electron from lattice site j to lattice site i, the t matrix $V_{l_1} G^f_{l_1,l_2}(z) V^*_{l_2}$ accounts for all the scattering processes of the conduction electrons on all the correlated impurity orbitals.

In the wide band limit, the influence of the host onto the dynamics of the correlated orbitals is determined by the real part and the imaginary part of $\boldsymbol{\Delta}_\sigma(z)$ at the Fermi energy [4].

In a first step, we diagonalize $\boldsymbol{\Gamma}_\sigma = \Im \boldsymbol{\Delta}_\sigma(-i0^+)$. The eigenvalues $\tilde{V}_l$ define the new couplings to N_f independent effective conduction bands [4], while the eigenvectors describe the composition of the new local orbitals in the rotated base.

The real part $\boldsymbol{T}_\sigma = \Re \boldsymbol{\Delta}_\sigma(-i0^+)$ contains the host-mediated effective hopping matrix element between the local orbitals, which are absorbed into the matrix $\boldsymbol{E}'_\sigma$,

$$\boldsymbol{E}'_\sigma = \boldsymbol{E}_\sigma + \boldsymbol{T}_\sigma, \tag{14}$$

and rotated into the new local operator eigenbasis,

$$\boldsymbol{E}''_\sigma = \boldsymbol{U}^h \boldsymbol{E}'_\sigma \boldsymbol{U}, \tag{15}$$

where the unitary matrix $\boldsymbol{U}$ is obtained from the diagonalization of $\boldsymbol{\Gamma}_\sigma$: $\text{diag}(\Gamma_\sigma) = \boldsymbol{U}^h \boldsymbol{\Gamma}_\sigma \boldsymbol{U}$.

This procedure defines a mapping of the original Hamiltonian, Eq. (5), onto an effective Hubbard model that couples to multiple effective conduction band channels:

$$\bar{H} = \sum_{ij,\sigma} \boldsymbol{E}''_{ij,\sigma} \tilde{f}^\dagger_{i\sigma} \tilde{f}_{j\sigma} + \sum_{ij,nm} \bar{U}_{ij,nm} \tilde{f}^\dagger_{i\sigma} \tilde{f}^\dagger_{j\sigma'} \tilde{f}_{n\sigma'} \tilde{f}_{m\sigma} + \sum_{n=1}^{N_f} \tilde{V}_n (\tilde{f}^\dagger_{n\sigma} \tilde{c}_{n\sigma} + \text{H.c.}) + \sum_{n=1}^{N_f} \sum_{\vec{k}\sigma} \epsilon_{\vec{k}\sigma n} \tilde{c}^\dagger_{\vec{k}n\sigma} \tilde{c}_{\vec{k}n\sigma}, \tag{16}$$

where $\tilde{f}_{j\sigma}$ annihilates an electron in the new eigenorbital basis of $\boldsymbol{\Gamma}_\sigma$, and $\tilde{c}_{n\sigma}$ denotes the annihilation operator of the local Wannier orbital of auxiliary conduction band n. The matrix elements $\bar{U}_{ij,nm}$ are obtained by expressing the original real-space orbitals in Eq. (3) in the eigenbasis of $\boldsymbol{\Gamma}_\sigma$. Since the effect of particle-hole asymmetry of the original conduction band is included in the transfer matrix $\boldsymbol{T}_\sigma$, the auxiliary n screening channels are modeled by a featureless particle-hole symmetric band with $\tilde{\rho}_n(\omega) = \Theta(D - |\omega|)(1/2D)$ and $\tilde{V}_n = \sqrt{2D\Gamma_n/\pi}$, where Γ_n is the nth eigenvalue of $\boldsymbol{\Gamma}_\sigma$. $2D$ denotes the conduction electron band width. For more details, see the original paper on the mapping, Ref. [4].

Obviously, this Hubbard model cluster already contains the antiferromagnetic part of the Ruderman-Kittel-Kasuya-Yosida (RKKY) interaction mediated by the conduction electrons.

Generically, a multiband model with N_f effective conduction electron channels is expected from the N_f eigenvalues of $\boldsymbol{\Gamma}_\sigma$. It turns out, however, that the encoded topology in $\boldsymbol{\Delta}_\sigma$ typically leads to a reduced rank of $\boldsymbol{\Gamma}_\sigma$ [4]. Since the upper bound of the rank is given by the number of $\vec{k}$ vectors on the Fermi surface of the host, the problem reduces to an effective two-band model for arbitrary geometries in $1d$, which makes the mapped MIAM fully accessible to the NRG.

Since the NRG always diagonalizes the rotated correlated orbital problem exactly in the first step, the complexity of the problem is essentially limited by the Hilbert space dimension of the correlated impurity problem. We are able to obtain very accurate NRG results up to $N_f = 7$ correlated sites with the

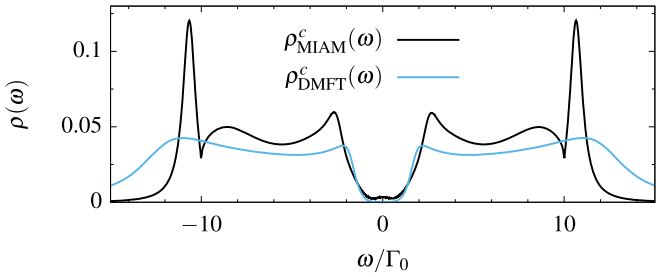

FIG. 2. c-spectral function for the central position in a $N_f = 7$ MIAM where $U = -2\epsilon_f = 10\Gamma_0$ in comparison with the DMFT solution of Kondo lattice model with the identical Kondo coupling $g = \rho J = \rho J_{\mathrm{SW}} = 0.25$ obtained by the Schrieffer-Wolff transformation [34].

computer facilities we have access to. We would like to refer the reader for more details on the approach and its limitation to our recent paper, Ref. [4].

The NRG applied to the mapped problem provides the correlation functions used to construct the correlation self-energy matrix according to Eq. (10) after rotating back into the real-space orbital basis. The full energy dependency of the uncorrelated host enters via Eq. (9) the f-orbital GF matrix. The equation of motion expression, Eq. (13), provides access to the real-space GF matrix at arbitrary lattice sites i, j that can be chosen independently of the location of the correlated orbitals. Essentially, the mapped MIAM serves as a powerful tool to calculate the real-space single-particle GF matrix including all spatial correlations of the original MIAM.

III. RESULTS

To set the stage for our detailed real-space investigation of the spectral functions in a finite-size MIAM, we plot a comparison between the c-orbital spectrum at the center, obtained via the exact equation of motion Eq. (13), and the conduction electron spectrum for a $1d$ Kondo lattice calculated within the DMFT [27] in Fig. 2. We set the local Kondo interaction in such a way that the dimensionless Kondo coupling $g = \rho J = \rho J_{\mathrm{SW}}$ agrees with the prediction of the Schrieffer-Wolff transformation, J_{SW} [34] in the MIAM.

The data clearly show excellent agreement between the DMFT and center spectra in the $N_f = 7$ cluster. The cluster spectrum contains all many-body intersite correlations exactly, which are only treated in mean-field within the DMFT. In addition, the NRG broadening is overestimated in the effective site of the DMFT, hence the MIAM spectrum is much sharper and contains subfeatures at higher energies which are absent in the DMFT. In addition, the DMFT shows a clear pseudogap with $\rho^c(\omega = 0) = 0$ while we observe a finite value $\rho^c(\omega = 0) > 0$ in the MIAM. This finite value can be explained within the extended Lieb-Mattis theorem as demonstrated later. In an infinitely large system, this finite value will disappear and the DMFT form will be asymptotically recovered.

For all NRG calculations, Λ denotes the NRG discretization parameter [26] and N_s labels the number of kept states after each NRG iteration.

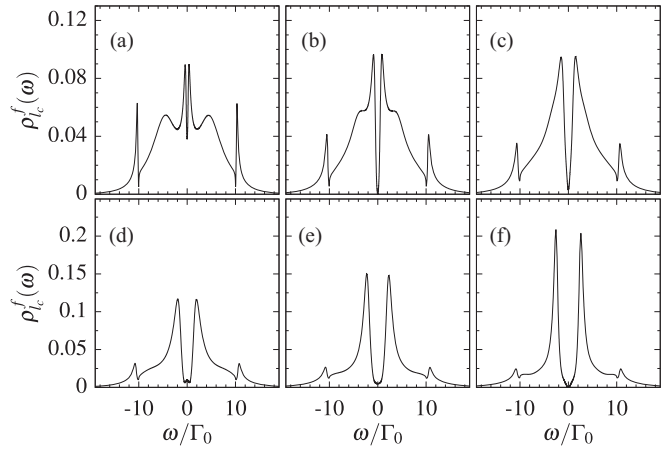

FIG. 3. Spectral function $\rho^f_{l_c}(\omega)$ of the central f orbital in a dense array comprising (a) $N^f = 2$, (b) $N_f = 3$, (c) $N_f = 4$, (d) $N_f = 5$, (e) $N_f = 6$, and (f) $N_f = 7$ impurities. In case of even N_f, both central f orbitals are equivalent due to parity symmetry. Parameters: $\epsilon_f = -U/2 = -5\Gamma_0$, $\epsilon^c = 0$, $D = 10\Gamma_0$, $\Lambda = 2$, and $N_s = 8000$.

A. Evolution of the center spectral function with the number of correlated sites N_f

We consider the geometry of Fig. 1 shown for $N_f = 7$ and vary the number of correlated sites from $N_f = 2$ to $N_f = 7$. The sites are labeled consecutively with $l = 1, \cdots, N_f$, $\epsilon_f = -U/2 = -5\Gamma_0$. The $1d$ conduction band host is particle-hole symmetric ($\epsilon^c = 0$) and the spectral functions are obtained by an NRG calculation with the parameters stated in the caption and by employing the algorithm [35,36] based on the complete NRG basis set [37,38].

The evolution of the spectral function at the center of the correlated sites, l_c, for $N_f = 2 - 7$ respectively, is shown in Fig. 3. The local spectral function at site l is extracted from the diagonal matrix element,

$$\rho^f_{l,\sigma}(\omega) = \frac{1}{\pi}\Im G^f_{ll,\sigma}(\omega - i0^+), \tag{17}$$

in the usual way. Note that we perform all calculations in the absence of an external magnetic field. Therefore, all spectra in this paper are spin independent. Although a magnetic order cannot occur in such a system with $N_f \leqslant 7$ according to the Mermin-Wagner theorem, the spin correlations induced by the RKKY interaction are revealed in the spin-correlation functions as extensively discussed in Refs. [4,24,39].

Let us first comment on the feature at $\omega \approx D = 10\Gamma_0$, visible in all spectra. This feature originates from the Van Hove singularity of the $1d$ density of states right at the band edge, which is included in $\mathbf{\Delta}(z)$, but doesn't have any further physical meaning. Hence we will ignore these discontinuities in the following discussion.

A common feature is the formation of a gap structure symmetrically around $\omega = 0$, whose width is increasing with N_f. This feature can be traced back to the spectral properties of a MIAM cluster by artificially setting $\mathbf{\Gamma}_\sigma = 0$ and only including $\boldsymbol{T}_\sigma = \Re\mathbf{\Delta}_\sigma(-i0^+)$ in an exact diagonalization. $\mathbf{\Gamma}_\sigma$ is responsible for the ferromagnetic component of the RKKY interaction [4], the remaining Kondo screening of a small

cluster spin moment [4], renormalization of parameters, and broadening of the spectrum.

We notice that $\rho_l^f(\omega=0)$ at the center location remains finite and only vanishes for $N_f=3$ and $N_f=7$. Particularly, the finding of a very small offset at $\omega=0$ raises the question of whether this feature is caused by a numerical problem or has a physical origin, since this has not been reported in $2d$ QMC spectra for a finite-size Kondo lattice cluster [22]. We show in the next section that this has a physical origin and the extended Lieb-Mattis theorem can be used to predict under which circumstances $\rho_l^f(\omega=0)=0$ and in which case $\rho_l^f(\omega=0)$ must be finite at $T=0$.

For $N_f=2$, we have a realization of a two-impurity model where the energy-dependent density of states break the particle-hole symmetry in the even and the odd channels [39–41], which generates the finite-size hopping between the two correlated sites [4,39]. We obtain two Kondo peaks, one in the even and one in the odd channel, that are shifted away equally and in an opposite direction from the chemical potential as a consequence of a nonresonant scattering. The symmetric superposition of the even and the odd spectral function yields the spectrum shown in Fig. 3(a). This spectrum develops a pronounced valley between the two peaks but with a finite density of states at $\omega=0$. The lower and upper charge excitations, sometimes referred to as Hubbard peaks, are well pronounced, as known from the SIAM.

In Fig. 3(b), we proceed to the center orbital of the $N_f=3$ cluster. Here we have the first MIAM of the second kind, where N_f exceeds the number of screening channels [4]. We have shown [4] that the LMs of the two outer orbitals are aligned and antiferromagnetic (AF) correlated with the center spin. By inspecting the spectrum in the vicinity of the chemical potential, we find an exactly vanishing $\rho_{l_c}^f(\omega=0)=0$. Increasing the local cluster size to $N_f=4$ generates a small density of states, $\rho_{l_c}^f(\omega=0)>0$. This observation holds up to $N_f=6$. The pseudogap width increases as well as the peak height, and spectral weight is transferred from the Hubbard peaks to the sharper features close to the Fermi level. The f density of states resemble a band formation of the correlated orbitals by the effective hopping matrix $\boldsymbol{T}$, which asymptotically evolves in the heavy quasiparticles close to the Kondo insulator band gap [42]. For a cluster size of $N_f=7$, the spectral function depicted in Fig. 3(f) develops a true pseudogap with $\rho_{l_c}^f(\omega=0)=0$.

B. Applying the extended Lieb-Mattis theorem for predicting a pseudo-gap spectrum

We can combine an auxiliary Kondo problem with the extended Lieb-Mattis theorem [23,24] to decide whether the spectral function should have a finite value $\rho_l^f(0)$ at $\omega=0$ or not. Shen [23] have proven that for a number of N_f LMs coupled by a local AF exchange interaction to a half-filled system of conduction electrons on a bipartite d-dimensional lattice with $N_c \geqslant N_f$ sites, the ground state has a total S_z component of

$$S_z^{\mathrm{tot}} = \tfrac{1}{2}|N_{c,\mathrm{A}} - N_{c,\mathrm{B}} + N_{f,\mathrm{B}} - N_{f,\mathrm{A}}|. \tag{18}$$

The extended version [24] generalizes Shen's version of the Lieb-Mattis theorem to predict the ground-state multiplet of a MIAM in the continuum limit, where the number N_c of c orbitals is considered to be infinitely large, $N_c \to \infty$. Thereby, a finite-size cluster is embedded into a conduction band continuum to account for a possible Kondo screening of cluster ground-state multiplets.

Setting aside subtle details of the spectrum close to $\omega=0$, the presented data in Fig. 3 suggest qualitatively parametrizing the density of states by a power-law fit $\rho_l^f(\omega) \approx \rho_l^f(0) + C_l|\omega|^r$ with an offset $\rho_l^f(0)$ and some exponent $r > 1/2$.

Let us imagine we extend the MIAM by an additional spin $1/2$ that is locally coupled antiferromagnetically with an arbitrarily weak Kondo coupling constant to the spin in the correlated orbital at site l. If the density of states is finite at $\omega=0$, a Kondo screening of this additional spin must occur in the limit $T \to 0$, and a strong coupling (SC) FP with a singlet ground state is found. If, however, $\rho_{l,\sigma}^f(0)=0$ and $r \geqslant 1/2$, we are dealing with a pseudogap Kondo problem [43–45] where theLM FP is stable in our parameter regime for $T \to 0$.

Since the ground state of the total system remains independent of the auxiliary AF coupling strength, we can now send the auxiliary coupling to infinity, creating a local singlet from the auxiliary spin and the LM at site l, such that the location of the fictitiously induced LM is shifted into the remaining system [24,46,47].

The essence of this first step is to map the problem of a finite spectral function $\rho_l^f(0)$ onto the question of a LM formation in an effective MIAM where the correlated site l has been removed. We extensively studied this so-called Kondo hole problem in a recent paper [24] where we have shown that the nature of the ground state can be derived from an extended Lieb-Mattis theorem on a bipartite lattice with AF couplings at half filling.

In a second step, we employ Shen's cluster Lieb-Mattis theorem [23] for a finite-size effective MIAM cluster [23,47] with the f orbital at site l being removed to determine its maximal spin component S_z^{tot} of the ground state. If $S_z^{\mathrm{tot}}=0$, no effective moment remains and $\rho_l^f(\omega=0)>0$.

If, however $S_z^{\mathrm{tot}}>0$, we have to be more careful and need to check in a third step whether by enlarging the conduction electron cluster, S_z^{tot} is increasing or decreasing, as outlined in Ref. [24]. This step extends finite-size clusters to a true continuum model including additional screening channels due to the coupling to the host conduction electrons. If S_z^{tot} increases, the effective exchange coupling of the ground-state spin multiplet to the remaining conduction band channels is ferromagnetic and a local moment prevails leading to $\rho_l^f(\omega=0)=0$. If, however S_z^{tot} decreases, we can conclude that the finite-size cluster is AF coupled to the effective conduction band channel and a singlet ground state is found in the Kondo hole problem.

A specific example where this procedure agrees perfectly with well-known and established theoretical as well as experimental results is the case of graphene. Here the bipartite lattice structure in combination with moderate correlations within the π-orbital enable the applicability of the Lieb-Mattis theorem, which predicts a stable local moment when a single carbon atom is removed. This is in agreement with theoretical studies on a microscopic level [48–50] and has already been observed experimentally [51–53]. At the same time, the

pseudogap in the density of states of pristine graphene with an exponent of $r = 1$ is well established as well, and the breakdown of the single ion Kondo effect was experimentally observed [52]. Hence, this example is in line with our argumentation that the occurrence of a stable LM when a single site is removed is directly related to a local pseudogap spectrum with exponent $r \geqslant 1/2$.

Moreover, the predictions of the auxiliary model also fit to the f-orbital spectra of a half filled $2d$ PAM on a simple cubic lattice with one f orbital being removed, see Fig. 5 of Ref. [54]. According to the Lieb-Mattis theorem, removing another f orbital on the same sublattice as the first one would increase the degeneracy of the ground state, whereas it is reduced when an f orbital on the opposite sublattice gets removed. Consequently, the spectra of the f orbitals on the opposite sublattice as the hole sites are expected to be finite at $\omega = 0$, while the others should be fully gapped. Note that the precise value of $\rho^f(\omega = 0) > 0$ cannot be predicted by the Lieb-Mattis theorem. It is expected that $\rho^f(\omega = 0) > 0$ falls rapidly with increasing distance from the hole site, such that it might be difficult to resolve for larger distances as shown in Fig. 3 of Ref. [54].

We applied the extended Lieb-Mattis theorem to the situation where we removed the correlated orbital at the center position l_c for the different cluster sizes N_f. Indeed, we only found a LM FP for $N_f = 3$ and $N_f = 7$, confirming our numerical findings as depicted in Fig. 3. For $N_f = 2$, the auxiliary problem reduces to a SIAM that has a singlet ground state, and, consequently, $\rho_1^f(\omega = 0) > 0$.

For $N_f = 3$, the Kondo-hole cluster yield $2S_z^{\rm tot} = 1$; adding another conduction electron site yields $2S_z^{\rm tot} = 2$, indicating a ferromagnetic coupling so the ground state carries a LM. It is interesting to note that this $N_f = 3 - 1 = 2$ effective Kondo-hole MIAM is identical to a two-impurity Anderson model with both impurities located on the same sublattice. For this case, we have explicitly proven in a NRG calculation including the full energy dependency of the conduction band host that the LM FP is stable [41]. Therefore, $\rho_2^f(\omega = 0) = 0$, for $N_f = 3$ as observed in Fig. 3(b).

Note that the $N_f = 3$ cluster is the minimal model to realize a MIAM of the second kind in a $1d$ host. In a MIAM of the second kind, the number of screening channels is less than the number of f orbitals [4], which is required to realize a fully gapped spectra. In Sec. III.1 of Ref. [24], we presented a detailed analysis for the noninteracting limit of the simplest realization for a MIAM of the second kind in arbitrary dimensions on a simple cubic lattice, arranged as schematically depicted in Fig. 6 of Ref. [24] for the $1d$ and $2d$ cases. The even parity subspace of the model contains the central f orbital (f_{l_c}) and the even linear combination of the outer ones ($f_+ \propto \sum_{i \neq l_c} f_i$). At low temperatures, only the center orbital, f_{l_c}, couples to the conduction band electrons, while the f_+ orbital does only indirectly couple via a finite hopping element t_{l_c+} between the f_{l_c} and f_+ orbitals. The GF of the f_{l_c} orbital now involves propagations into the (decoupled) f_+ orbital and back, which, in case of PH symmetry, results in a diverging real part of the self-energy $\propto t_{l_c+}^2/\omega$ and, consequently, in a fully gapped spectra—see Eq. (48) in Ref. [24]. Since this contribution to the self-energy is still present when the correlations are switched on, the spectra in these models will always be fully gapped. This argumentation also holds in $2d$ when $N_f = 5$ f orbitals are considered and arranged as depicted in Fig. 6(b) of Ref. [24]. In the $2d$ QMC study of Raczkowski and Assaad [22], however, no fully gapped spectrum was found for this specific $N_f = 5$ model—see Fig. 3(a) in Ref. [22]. We believe that the mismatch is a finite temperature effect, and encourage the authors of Ref. [22] to adopt the zero temperature project QMC algorithm so as to investigate in more details the long imaginary time behavior of the local $\tilde{f}$ GF.

For $N_f = 4$, a removal of the $l = 2$ f-orbital yields $2S_z^{\rm tot} = 1$. By extending the cluster with one conduction electron site [24] we can show that one of the two screening channels is AF coupled and, therefore, the ground state of the extended Kondo-hole MIAM cluster has a singlet ground state. We leave it to the reader to apply the extended Lieb-Mattis theorem to show that this prevails for $N_f = 5, 6$ while for $N_f = 7$ a finite LM FP is predicted by the Lieb-Mattis theorem which is compatible with our finding of $\rho_4^f(\omega = 0) = 0$ for $N_f = 7$.

The extended Lieb-Mattis theorem has turned out to be a very powerful tool to rigorously establish the ground state degeneracy of auxiliary MIAM, and allows us to make a prediction whether $\rho_l^f(\omega = 0)$ is finite or must vanish, independent of the selected numerical approach for the calculation of the spectral functions. This establishes the high accuracy of our NRG calculations presented in Fig. 3, which are fully compatible with the prediction of the extended Lieb-Mattis theorem.

C. Concentrated MIAM cluster with $N_f = 7$

This section is devoted to the investigation of the real-space spectral functions for a MIAM cluster depicted in Fig. 1.

1. Real-space spectral functions

After establishing the evolution of the spectral function at the central site with the cluster size N_f, we investigate the site-depending spectra for our largest MIAM with $N_f = 7$. We present the f spectra for the correlated site $l = 1, 2, 3$ and the center location $l_c = 4$ in Figs. 4(a)–4(d). Note that the data shown in Fig. 4(d) are identical to Fig. 3(f) and are added for completeness.

A pseudogap feature is found in the spectra of all sites with two nearest neighbors. This pseudogap is absent on the surface of the correlated chain, i.e., at $l = 1$ and $l = N_f$, which resembles more of a SIAM-type spectral function. Since this feature has also been reported by Raczkowski and Assaad [22] in an auxiliary QMC calculation for a $2d$ Kondo cluster model on a substrate, we believe this is a generic surface property of a finite-size MIAM in arbitrary spatial dimensions.

We can resort to the extended Lieb-Mattis theorem exemplified in our small clusters, that such metallic surface spectrum must indeed prevail in arbitrary spatial dimensions and cluster sizes N_f, as long as the number N_c of lattice sites of the underlying metallic host is always significantly larger, $N_c > N_f$. By removing an arbitrary correlated orbital on the surface of the cluster, we are left with a new dense cluster of size $N_f - 1$ which again has a singlet ground state. The neglected coupling to the rest of the host does not change

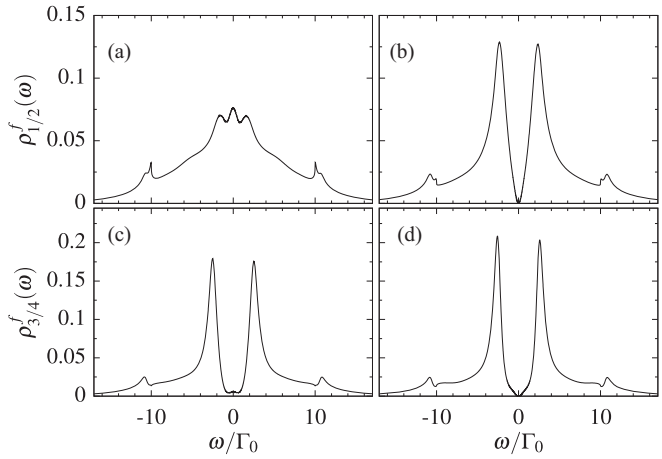

FIG. 4. Spectral functions $\rho^f(\omega)$ for an impurity array comprising $N_f = 7$ f orbitals. The panels depict the spectral function of the individual f orbitals starting at the outermost in panel (a) and ending at the center in panel (d). Parameters as in Fig. 3.

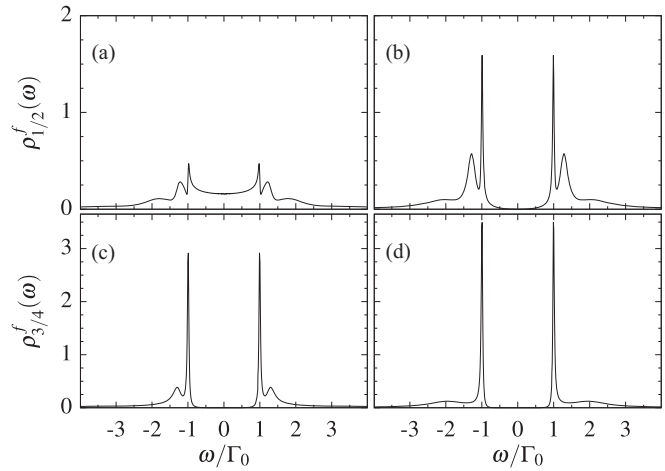

FIG. 5. Effective spectral functions $\tilde{\rho}^f(\omega)$ for an impurity array comprising $N_f = 7$ uncorrelated f orbitals that are located at $\epsilon^f_l = 0$ to maintain half filling. The panels depict the spectral function of the individual f orbitals starting at the outermost in (a) and ending at the center in panel (d).

the ground-state property. The screening of an auxiliary spin coupled antiferromagnetically to a surface f orbital is always possible and, therefore, the density of states of the correlated orbital at the surface for $\omega = 0$ must always remain finite. This general statement provides an explanation for the finite f-spectral function $\rho^f(\omega = 0)$ at the surface of 6×6 Kondo cluster model [22] and in our $1d$ correlated chain.

Let us proceed to the other correlated sites l with $1 < l < N_f$. At $l = 2$ and $l_c = 4$, $\rho^f_l(\omega = 0)$ vanishes exactly, while we find $\rho^f_l(\omega = 0) > 0$ for $l = 1, 3$ in the data presented in Fig. 4. Again, this observation is consistent with the prediction of the extended Lieb-Mattis theorem. Since the number of uncorrelated sites are fixed and have an imbalance of 1 for $N_f = 7$, $S^{\rm tot}_z$ of the MIAM cluster obtained from Eq. (18) is independent of the sublattice of the removed correlated orbital, and we always find $S^{\rm tot}_z = 1/2$. The cluster develops a LM ground state as expected from the isolated Kondo-hole problem [24]. Now we add one more uncorrelated orbital which must belong to the opposite sublattice as the first or last lattice site of the cluster. While this leads to $N_{c,A} - N_{c,B} = 0$, the total spin of the extended cluster depends on the imbalance $N_{f,B} - N_{f,A}$. Without loss of generality, let us assume that l odd belongs to sublattice A. If we remove a correlated f orbital on sublattice A, we obtain $S^{\rm tot}_z = 0$, and consequently a finite $\rho^f_l(\omega = 0)$, while for even l that belongs to sublattice B, the ground-state spin is increasing to $S^{\rm tot}_z = 1$. Consequently, the effective MIAM cluster ground-state spin is ferromagnetically coupled to the host for removing an l even correlated orbital and the LM cannot be fully screened. At these lattice sites, $\rho^f_l(\omega = 0)$ must vanish, confirming the findings of our NRG calculation.

The magnitude of $\rho^f_l(\omega = 0) > 0$, however, is not determined by the extended Lieb-Mattis theorem. To provide a basic understanding of the density of states, we assume that the MIAM cluster shows FL properties for $T \to 0$, implying that we can replace the full self-energy matrix $\mathbf{\Sigma}_\sigma(z)$ in Eq. (9) for $z \to 0$ by the Hartree contribution $\Re[\mathbf{\Sigma}_\sigma(0)]$. The diagonal matrix elements renormalize the local single-particle $\epsilon^f_l \to \epsilon^f_l + U/2 = 0$ to ensure half filling. The off-diagonal matrix elements renormalize the hopping matrix $\boldsymbol{T}$ but its magnitude is analytically not known. Therefore, we calculated the spatially dependent spectral functions from $\tilde{\boldsymbol{G}}^f_\sigma(z) = [z - \mathbf{\Delta}_\sigma(z)]^{-1}$ in Fig. 5 by neglecting the finite U off-diagonal Hartree terms, essentially defining the $U = 0$ and $\epsilon^f_l = 0$ problem.

Interestingly, the surface spectrum $\rho^f_{1,\sigma}(\omega = 0)$ remains metallic while all bulk spectral functions develop a finite gap. This gap corresponds exactly to the analytic gap of the $1d$ PAM located at $\pm\Gamma_0$. This confirms that a metallic surface and bulk gap-formation is already present in the $U = 0$ PH symmetric MIAM. In the corresponding local conduction electron spectra calculated by the exact equation of motion in Eq. (13), we found fully gapped spectra for all uncorrected conduction electrons at the sites l—not shown here.

We still need to reconcile the even-odd oscillations in $\rho^f_l(\omega = 0)$ for $U > 0$ with the finding of a gap for all bulk sites $1 < l < N_f$ when $U = 0$. A more careful analysis presented in Ref. [24] relates that to a $U = 0$ Kosterlitz-Thouless-type transition in the model where the f orbital at site l has been removed. To elaborate on this difference, we still use the auxiliary spin picture for probing the local f spectrum and employ the $U = 0$ supercell analysis for the MIAM presented in Ref. [24].

In an isolated cluster of noninteracting orbitals and half filling, we have shown that removing a single f-orbital at site $1 < l < N_f$ generates a localized state. For a nearest-neighbor tight-binding model, this localized orbital is located at the neighboring f sites and at the conduction band Wannier orbital l [24]. Therefore, the f-electron spectra must have a gap which we interpret as a precursor of the bulk gap.

Now we switch on a finite U. As we have demonstrated in Ref. [24], the localized bound single-particle orbitals can acquire a U-induced effective Kondo coupling such that the low-temperature LMs are screened at $T = 0$. This provides

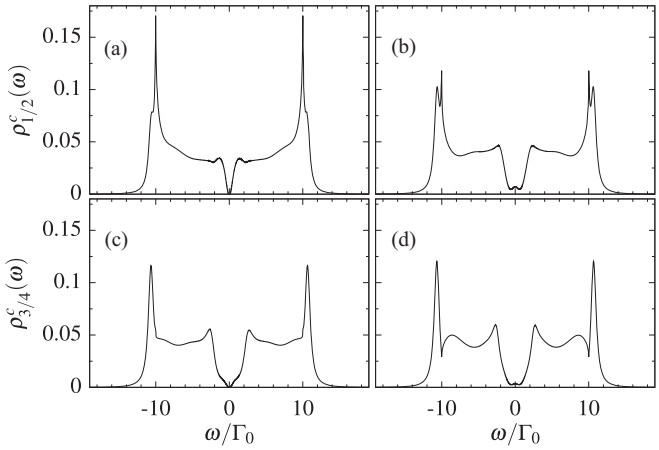

FIG. 6. The conduction electron spectral functions $\rho^c_l(\omega)$ for the same parameters as in Fig. 4(a) $l = 1$, (b) $l = 2$, (c) $l = 3$, (d) $l = 4$, The Green's functions were calculated via Eq. (13).

the microscopic mechanism that is implicitly accounted for by the extended Lieb-Mattis theorem which is only valid for $U > 0$ and half filling. Since this effective Kondo coupling increases with some power law U^α, $\alpha > 1$ [24] for small U, this mechanism also explains that the zero frequency peaks for $U/\Gamma_0 = 20$ as shown in Fig. 7 are larger than those in Fig. 4 for $U/\Gamma_0 = 10$. Eventually, for very large U, the crossover temperature T_0 at which the LM is screened will decrease again as depicted in Fig. 15 of Ref. [24].

Since the effective Kondo coupling for screening the LM depends on its distance from the edge, this mechanism is increasingly suppressed when moving from the edge to the center (bulk). Therefore, the pseudogap becomes more pronounced, and the finite $\rho^f_l(\omega = 0)$ is reduced beyond detectability for large cluster sizes $N_f \to \infty$, even when the extended Lieb-Mattis theory predicts $\rho^f_l(\omega = 0) > 0$.

Since the dimensionality of a cluster does not enter the theorem, we expect that such A-B sublattice oscillations in the local f spectra should also be present in a $2d$ Kondo cluster for $U > 0$. Raczkowski and Assaad [22], however, do not address this question, and the presented data in Fig. 3 of

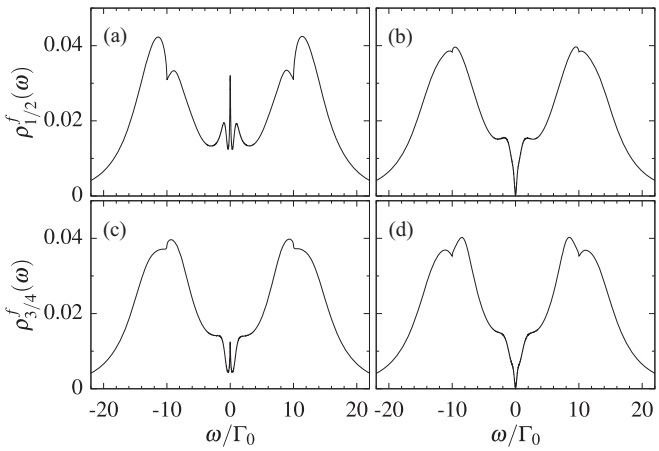

FIG. 7. Same as in Fig. 4 but with $\epsilon_f = -U/2 = -10\Gamma_0$.

Ref. [22] suggests a true pseudogap away from the cluster surface. This might be linked to the limits of the employed auxiliary QMC. In our NRG calculations, we had to access exponential small temperature scales well below the single impurity Kondo temperature to reveal these A-B sublattice oscillations in the f spectra.

Also note that the extended Lieb-Mattis theorem cannot make a prediction of the magnitude of $\rho^f_l(\omega = 0)$ and only can help distinguishing between a finite $\rho^f_l(\omega = 0)$ and $\rho^f_l(\omega = 0) = 0$.

Setting aside the even-odd oscillations of $\rho^f_l(0)$, we clearly can recognize the evolution of the spectral function from an impurity type spectrum more towards a bulk spectrum with a well pronounced pseudogap that is compatible in width with the DMFT solution of the $1d$ Kondo lattice problem.

In Fig. 6, we present the spectra for the corresponding conduction electron orbital at cluster site l. The GF was calculated via Eq. (13). The Van Hove singularities of the $1d$ simple cubic density of states of the host at the band edges are clearly visible. Additionally, a gaped density of states is also found at the surface of the cluster. This is for arbitrary N_f and is in agreement with the findings in Ref. [22]. Note that the data of Fig. 6(d) was already used for the comparison between the DMFT Kondo lattice solution and the cluster calculations as presented in Fig. 2.

Reminiscence of the Hubbard side peaks expected at $\omega \approx \pm U/2$ in the spectra can only be seen for $l = 1$ in Fig. 4, while they disappeared for $1 < l < N_f$. We attribute this to the strongly energy dependent self-energy matrix $\mathbf{\Sigma}(z)$ as well as the peculiar feature of a $1d$ density of states that is included in $\mathbf{\Delta}_\sigma(z)$ which shows square-root-type divergencies at both band edges.

We can, however, recover the Hubbard side peaks by increasing U. The spectral functions for $U = 20\Gamma_0$ are shown in Fig. 7 using the same NRG parameters as in Fig. 4. For each of the calculations, we have used adequate NRG iterations such that the spectrum remains unaltered when increasing the number of iterations to ensure that we are well in the low-temperature FP and $T \to 0$.

In addition, a low-energy Kondo peak emerges on odd lattice sites. The hopping matrix $\boldsymbol{T}_\sigma$ generates an antiferromagnetic coupling of the different cluster LMs which leave a $S = 1/2$ ground-state multiplet. The bulk gap is already seen in the ED spectrum of the cluster. The remaining coupling to the conduction electron bands causes the Kondo screening of this spin 1/2 ground state, leading a very narrow Kondo peak in the preformed gap structure at odd cluster sites.

2. Discussion: Metallic surface conductor in an Kondo insulator

So far, we exemplified a metallic surface f spectra in a small MIAM cluster embedded in a metallic environment that is in agreement with auxiliary field QMC data [22] as well as with the extended Lieb-Mattis theorem. Since the spatial dimension does not enter in the extended Lieb-Mattis theorem, only requiring half filling, antiferromagnetic coupling and a bipartite lattice, we can conclude that even the surface of a macroscopically large cluster in 3D will be a surface conductor as long as the number of host lattice sites $N_c \gg N_f$.

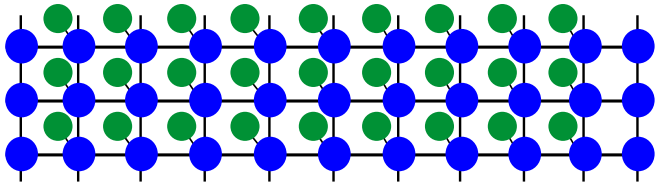

FIG. 8. Sketch of a strip of a $2d$ MIAM model for a Kondo insulator with a infinite large y axis but a finite-size x axis to define a surface. The correlated orbitals are depicted in green, the uncorrelated in blue. Note that on the surface the correlated orbitals are absent.

On the other hand, we can use the cluster Lieb-Mattis theorem [23] to analyze the surface states of a very large but finite-size cluster where $N_f = N_c = O(10^{23})$. Since the removal of a single orbital, correlated or uncorrelated does not matter, always induces a LM of $s = 1/2$, the spectra must always have a gap independent of the boundary conditions. This well-known observation inspired many theoretical papers [17–20] in which the Kondo lattice model is extended by spin-orbit interactions to a topological Kondo insulator to address the experimental findings of a metallic surface conductance on Kondo insulators [11–13]. All these concepts use a perfect lattice structure that abruptly ends at some boundary which appears to be very unrealistic in real strongly correlated materials that often have changing surfaces after cleaving. Chemical reactions with oxygen or surface roughness leads to deviation of the surface for an ideal situation. This well-known fact made topological models so popular because a metallic surface state is topologically protected independent of the surface ruggedness of the real material.

This discrepancy between the ideal trivial Kondo lattice with its insulating surface and a generically metallic surface in a large Kondo lattice cluster model embedded in an infinitely large metallic host raises the question of how many additional uncorrelated orbitals we need to add to see a metallic surface state developing at the edge of the Kondo lattice.

For simplicity, let us consider a $2d$ strip of a Kondo insulator symbolized in Fig. 8. We imagine a very large system in the y direction with $N_y \to \infty$. The number of sites N_x in x directions remains finite to establish two $1d$ surfaces at both edges of the strip. The exact number N_x does not enter the argument and can be arbitrarily large but only needs to be finite to establish an edge. The major ingredient in the setup of Fig. 8 is the removal of the correlated orbital at the surface layer of a Kondo insulator. In essence, Fig. 8 describes the smallest extension of a pristine finite-size Kondo lattice model to a MIAM by adding a single uncorrelated orbital.

In the case of a finite N_y the conventional Lieb-Mattis theorem needs to be applied. In analogy to the conventional Kondo insulator, removing a single orbital always leads to a change of the ground-state multiplet and, hence, starting from $S_z^{\text{tot}} = 0$ results in $S_z^{\text{tot}} = 1/2$, indicating $\rho_l^{f/c}(\omega = 0) = 0$. To clarify the existence of a gapped f spectra at the boundary in the continuum limit $N_y \to \infty$, we invoke the arguments of the extended Lieb-Mattis theorem as outlined before. In a first step, we neglect the two edge stripes of uncorrelated orbitals such that the model results in the conventional Kondo insulator, and a $S_z^{\text{tot}} = 1/2$ ground state emerges after removing one of the f orbitals at an arbitrary site (not only at the boundary). However, after including the uncorrelated edge stripes, the extended Lieb-Mattis theorem predicts a reduction of the moment to $S_z^{\text{tot}} = 0$ which proves an effective antiferromagnetic coupling of the induced LM and the $1d$ edge strip when recovering the original model as depicted in Fig. 8: The ground state remains in the SC FP from which we conclude that all the f spectra must be metallic, $\rho_l^f(\omega = 0) > 0$.

Since we expect an exponential suppression of the metallic states in the bulk, that is, beyond the extended Lieb-Mattis theorem which only distinguishes between $\rho_l^f(\omega = 0) > 0$ and $\rho_l^f(\omega = 0) = 0$, this strongly indicates that even for an infinitely large system, adding a layer of uncorrelated orbitals immediately yields a metallic surface even in a conventional Kondo insulator.

Here the metallic behavior is driven by the Kondo effect, while the gap formation in the Kondo insulator is more related to a self-screening mechanism driven by the RKKY interaction than to a picture of a single ion Kondo effect.

This leaves the question of the role of the correlations and in more detail the properties of the uncorrelated surface orbital defining the two vertical surface boundaries in Fig. 8. By making use of the adiabatic connection of the ground-state properties upon varying the parameter strength, we can answer some aspects by sending the local hybridization $V_l \to \infty$. Then the correlated site forms individual bound states with the local conduction orbital comparable with an infinitely strong Kondo coupling. Consequently, two uncorrelated $1d$ surface tight-binding models emerge which show trivial metallic behavior determined by the tight-binding model of the edge states. This metallic behavior will be preserved for finite V_l and we end up with a trivial metallic surface for arbitrary V_l but with an unclear mixture of the different orbitals.

We tested this prediction by considering the mean-field theory, i.e., setting $\tilde{\epsilon}^f = \epsilon^f + U/2$ which is equivalent to $U = 0$ while maintaining particle-hole symmetry. We solved the single-particle tight-binding model in the geometry shown in Fig. 8 for an infinitely large stripe of width $N_x = 50$ with periodic boundary condition in y directions. The $2N_y - 2$ bands are depicted in Fig. 9(a) revealing an insulating behavior with a finite band gap. $N_y - 2$ bands lay completely below the chemical potential $\mu = 0$ and $N_y - 2$ bands are located above it.

In addition, two noncrossing metallic bands emerge as shown in the inset of Fig. 9(a). To identify the spatial location of the metallic band and the orbital content, we plot the probability contribution of the c-edge orbital at $l_x = 1$ or $l_x = N_x$ and the f-edge orbital at $l_x = 2$ or $l_x = N_x - 2$ in Fig. 9(b) as a function of the hybridization strength V at the chemical potential. The inset depicts the probability contribution for $V/t = 1$ as a function of l_x on a logarithmic scale. The data reveals that the metallic state is exponentially localized at the edge and V/t determines the mixture of c and f orbitals. For a small hybridization, the wide band limit, the f-orbital content dominates while with increasing V the uncorrelated edge orbital increases its contribution. For $V = t$, both orbitals contribute equally. The figure also confirms the prediction made above that for infinitely large V, only the uncorrelated

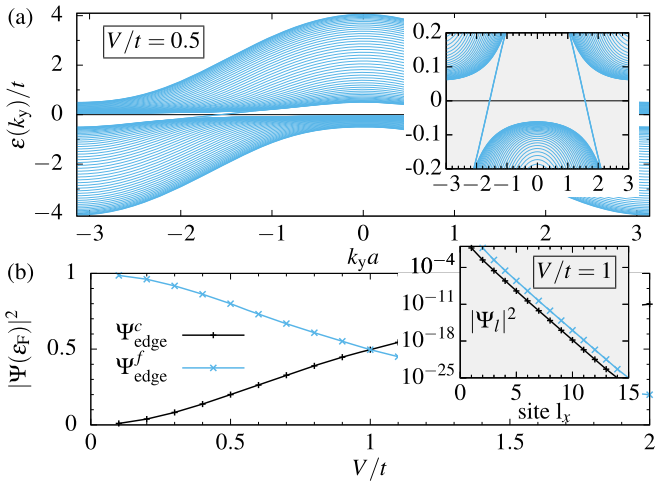

FIG. 9. (a) The k_y-dependent band structure for the periodic stripe in Hartree mean field theory, $\tilde{\epsilon}^f = \epsilon^f + U/2 = 0$ of a Kondo insulator model depicted in Fig. 8 and $V_l/t = 0.5$ for a stripe width of $N_x = 50$. The inset on the left-hand side reveals the small hybridization gap and the insulating behavior. Clearly visible are the two metallic surface bands that are not crossing each other, one for positive and one for negative k_y. (b) Probability of the edge f and c orbital contribution at the Fermi energy to the metallic band as function of V/t. The inset depicts this probability contribution for $V/t = 1$ as function of the site along the x axis on a logarithmic scale.

edge orbitals contribute to the metallic surface band close to the chemical potential. We conjecture that this picture prevails in a model that also includes the fluctuating contributions of the Coulomb interaction.

In addition, the inset in Fig. 9(b) also reveals that the local density of states $\rho^f_{l_x,l_y}(0)$ and $\rho^c_{l_x,l_y}(0)$ remain finite in agreement with the finite U extended Lieb-Mattis theorem. Our $U = 0$ analysis and the exponential localization of the metallic surface state in the bulk also reconciles the seeming paradox of the prediction of a finite spectra at $\omega = 0$ by the extended Lieb-Mattis theorem and the expectation of a bulk insulator. The contribution of the metallic surface band to the bulk spectrum at $\omega = 0$ becomes exponentially small, and for practical purposes one cannot distinguish the bulk spectra from a true insulator with vanishing spectra at $\omega = 0$. Since the results for the $U = 0$ spectra are in line with the finite U prediction, there is no QPT at $U = 0$ in this case, which we attribute to geometric differences between infinite and semi-infinite $2d$ systems. The supercell analysis in Ref. [24] is valid in arbitrary dimensions, but relies on periodic boundary conditions in all spatial directions.

D. Real-space spectral functions for the Kondo-hole problem

In this section, we address the question how a Kondo-hole located at the center of a $N_f = 7$ MIAM cluster changes the spectral properties. The geometry of the problem is sketched in Fig. 10. We replace the center f orbital by an uncorrelated orbital with a single-particle energy $\epsilon^f_{l_c} = \epsilon^h$ and $U_{l_c} = 0$. This allows for modeling charge neutral substitution of Ce by La, which has a finite $4f$ orbital energy $\epsilon^h \geqslant 0$ up to complete removing the site by setting $\epsilon^h \to \infty$ [24].

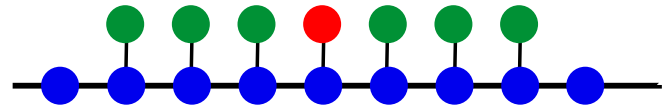

FIG. 10. Sketch of the geometric setup with a Kondo hole: An array of $N_f = 7$ correlated f orbitals (green) are locally coupled to a $1d$ tight-binding chain (blue) with $N_c \gg N_f$. We replace the center correlated orbital with one uncorrelated orbital (red) and introduce ϵ^h as its single orbital energy.

Let us start with the evolution of the spectrum at the outermost f orbital for six different values ϵ^h/Γ_0 plotted in Fig. 11. The initial cluster occupation starts out at $N_f = 7$ charges at $\epsilon^h/\Gamma_0 = 0.0$ and monotonically decreases to six charges for $\epsilon^h \to \infty$ when the central orbital is completely unoccupied and can be removed. Therefore, we expect that spectral weight is shifted from $\omega < 0$ to $\omega > 0$ upon increasing ϵ^h. The main shift of the spectral weight is expected to occur for the central orbital.

The system undergoes a QPT [24] at critical value $\epsilon^h_c/\Gamma_0 \approx 2.25$ from a SC FP for $|\epsilon^h| < \epsilon^h_c$ to a LM FP for $|\epsilon^h| > \epsilon^h_c$ in agreement with the extended Lieb-Mattis theorem. The initial PH symmetric spectrum becomes PH asymmetric for $\epsilon^h > 0$. The screening temperature T_0 is exponentially suppressed at ϵ^h_c, typical for a Kosterlitz-Thouless-type transition, and the very narrow Kondo peak developing at $\omega = 0$ becomes numerically not resolvable when approaching the QPT, i.e., $\epsilon^h \to [\epsilon^h_c]^-$. However, the boundary or surface spectrum remains metallic at any time.

The situation changes when inspecting the spectral evolution for the second correlated orbital $l = 2$ as depicted in Fig. 12 for the same parameters as in the previous figure. As in Fig. 4(b), the spectra vanishes at $\omega = 0$ for $\epsilon^h = 0$ [55]. Also, the extended Lieb-Mattis theorem is not applicable for finite ϵ^h since the system is shifted away from half filling.

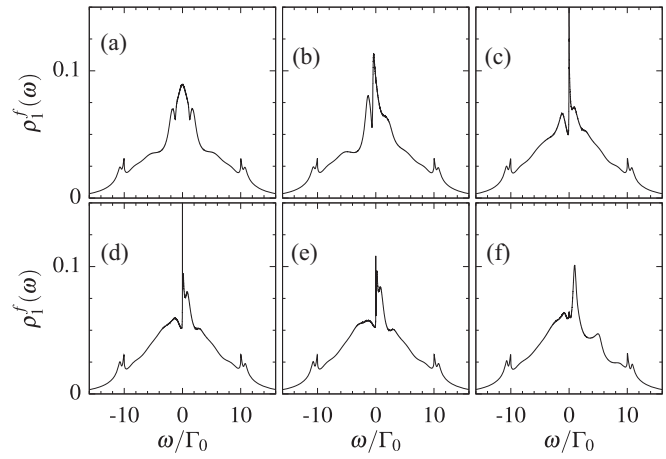

FIG. 11. Spectral function of the outermost f orbital in an $N_f = 7$ impurity array with an uncorrelated hole orbital in its center at $\epsilon_c = 0$. For the correlated f orbitals, $\epsilon_f = -U/2 = -5\Gamma_0$ holds, and the different panels show different on-site energies of the hole orbital: (a) $\epsilon^h/\Gamma_0 = 0.0$, (b) $\epsilon^h/\Gamma_0 = 1.0$, (c) $\epsilon^h/\Gamma_0 = 2.0$, (d) $\epsilon^h/\Gamma_0 = 2.1$, (e) $\epsilon^h/\Gamma_0 = 2.2$, (f) $\epsilon^h/\Gamma_0 = 5.0$. The QCP occurs at around $\epsilon^h_c/\Gamma_0 \approx 2.25$.

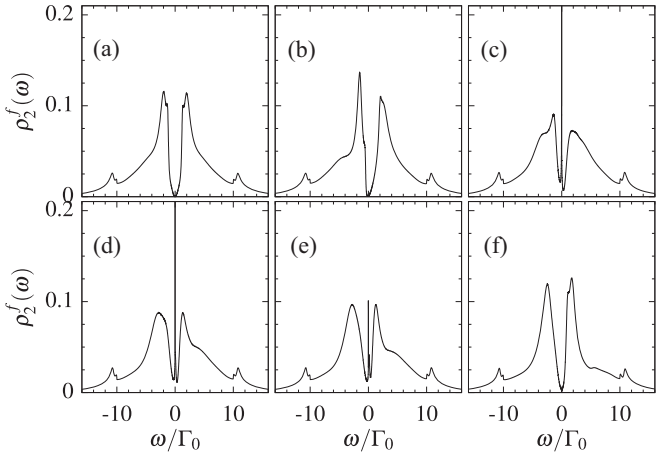

FIG. 12. Same as Fig. 11 but for the second f orbital.

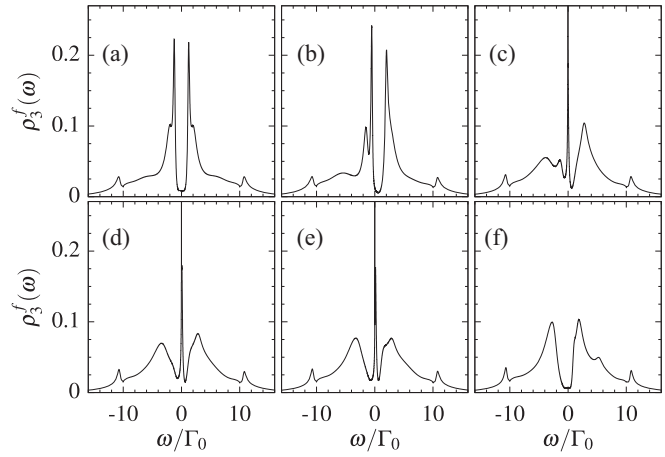

FIG. 13. Evolution of $\rho^f_{3,\sigma}(\omega)$ neighboring the hole site for the same parameters as in Fig. 11.

A quasibound state is developing at the two adjacent sites to the Kondo hole, $l = 3$ and $l = 5$, whose LM is screened via a coupling mediated by the central uncorrelated Kondo hole orbital. Once the low-energy (Kondo) scale is small enough, a very narrow Kondo peak develops inside the gap, as can be seen in Fig. 12(c). Furthermore, the pseudo-gap is absent,and $\rho^f_{2,\sigma}(0) > 0$. This additional Kondo effect well below the coherent temperature of the $N_f = 7$ cluster destroys the Kondo insulator properties in the spectra. The system approaches the KT-type QPT when increasing $\epsilon^h \to \epsilon^h_c$. The low-temperature screening scale is already exponentially suppressed in Fig. 12(e) such that the peak is very hard to resolve. In the LM phase, depicted in Fig. 12(f), the Kondo peak is absent in the spectrum, leaving us with a slightly asymmetric spectrum with an onset of a pseudogap. For $\epsilon^h \to \infty$, we recover a half-filled system with one correlated site removed. The extended Lieb-Mattis theorem predicts a true pseudogap spectrum with $\rho^f_{2,\sigma}(0) = 0$, consistent with the spectrum in the LM phase as depicted in Fig. 12(f). Note, however, that $\rho^f_{2,\sigma}(0)$ is very small at finite ϵ^h and only vanishes in the limit $\epsilon^h \to \infty$ where the extended Lieb-Mattis theorem is applicable.

Figure 13 shows the evolution of spectra for the third side using the same parameters as in the previous two figures. On top of a spectral valley around $\omega = 0$ with $\rho^f_{3,\sigma}(0) > 0$, a Kondo peak emerges at $\omega = 0$ due to the screening of LM that is created by the Kondo hole as long as $\epsilon^h < \epsilon^h_c$. This Kondo peak also disappears at the QPT once we enter the LM regime. However, an additional finite frequency peak is clearly visible at finite but small ω in the spectral function plotted in Fig. 13(f) whose origin we discuss below.

With this basic understanding of spectral evolution, we draw our attention to the spectrum at the Kondo-hole site hosting an uncorrelated f orbital whose single-particle energy is increased across the KT-type transition in the panels from Figs. 14(a)–14(f) using the same parameters as for the previous three figures. Starting from a PH symmetric spectrum with a gap, i.e., $\rho^f_{4,\sigma}(0) = 0$, for $\epsilon^h = 0$, the spectrum becomes increasingly more asymmetric and the gap disappears. We also observe the substantial shift of the spectral weight from below to above the chemical potential, reflecting that the Kondo-hole occupations are rapidly and monotonically decreasing for $1 < \epsilon^h/\Gamma_0 \to \infty$. In fact, the crossover from half filling to an empty orbital occurs just before ϵ^h_c but does not coincide with the QPT.

Starting from Fig. 14(c), the main single-particle spectral peak from the local orbital is clearly visible at $0 < \omega \approx \epsilon^h$. Simultaneously, the spectrum shows an additional peak that crosses the Fermi energy just below the critical value ϵ^h_c. Its spectral contribution is small and is overshadowed by a very narrow Kondo resonance that disappears in the LM regime depicted in Fig. 14(f).

To address the spectral evolution across the QPT in more detail, we focus on the low-energy part of the site-dependent spectra for three values $\epsilon^h/\Gamma_0 = 2.1, 2.2, 2.3$ and combine the three spectra for each cluster site into one panel of Fig. 15, starting from the outermost site $l = 1$ in Fig. 15(a) and ending at the center site $l_c = 4$ plotted in Fig. 15(d). We clearly see the Kondo resonances at each site pinned at $\omega = 0$, which is a result of the screening of the cluster LM. The peak height depends on the contribution of the local site to this Kondo effect, and the resonance is absent in the LM FP.

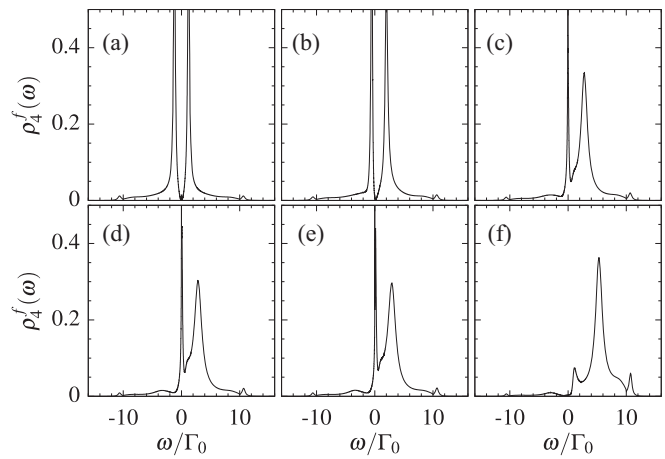

FIG. 14. Evolution of the Kondo hole spectrum $\rho^f_{4,\sigma}(\omega)$ in the cluster center for the same parameters as in Fig. 11.

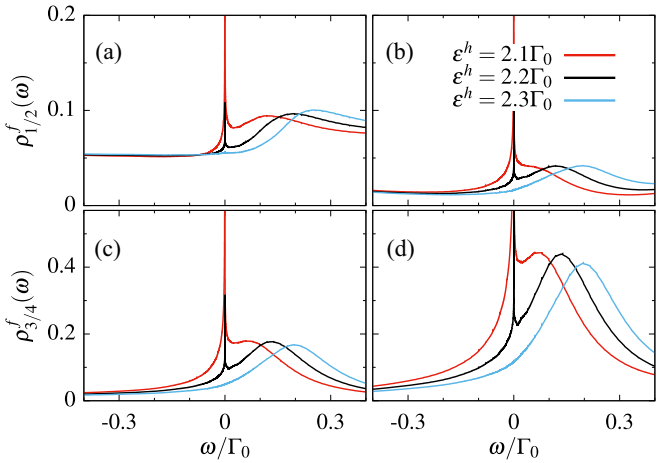

FIG. 15. Zoom of the spectral functions around the Fermi energy near the QCP located at $\epsilon^h_c/\Gamma_0 \approx 2.25$. (a) $l = 1$, (b) $l = 2$, (c) $l = 3$, (d) $l = l_c = 4$.

In addition, we observe a broader resonance just above the Fermi energy most pronounced in the spectra around the Kondo hole as plotted in Figs. 15(c) and 15(d). To clarify its origin, we performed an exact diagonalization of the MIAM Kondo-hole cluster by just taking into account the intersite hopping generated by $\boldsymbol{T}_\sigma = \Re\boldsymbol{\Delta}_\sigma(-i0^+)$ and ignoring the coupling to the effective band continua, setting $\boldsymbol{\Gamma}_\sigma = 0$. It turns out that upon raising of ϵ^h, a low-lying excitation in the spectrum is crossing the Fermi energy and simultaneously the cluster occupation on the f sites decreases from $N = 7$ to $N = 6$ charges. This sharp cluster excitation is broadened by including the hybridization $\boldsymbol{\Gamma}$ to the broader peaks located around $0.1 < \omega/\Gamma_0 < 0.3$. Therefore, this is a contribution from a collective excitation within the effective MIAM cluster.

The QPT, however, does not occur exactly at this mixed valence point between $N = 6$ and $N = 7$: It is energetically more favorable to form a SC FP and pay some extra single-particle energy ϵ^h as long as the energy gain in spin screening energy as well as the gain in hybridization energy is larger than the energy loss by the virtual occupation of the Kondo-hole orbital. Such behavior is typical for a QPT changing the ground-state degeneracy and has been discussed in the context of a chemically driven QPT in a two-molecule Kondo system [56]. This energy argument explains why the orbital peak and the peak of low-lying cluster excitation is observed at $\omega > 0$ and a Kondo effect is still formed.

IV. CONCLUSION

In this paper, we studied the spectral properties of dense $1d$ MIAMs comprising up to $N_f = 7$ correlated orbitals using NRG in combination with a recently developed wide band approximation [4]. We focused on the parameter regime with a half-filled conduction band such that the model describes a Kondo insulator in the limit $N_f \to \infty$ when maintaining PH symmetry.

Increasing N_f, a dip in the spectra of the central sites develops rapidly, already leading to a full gap for $N_f = 3$. This rapid onset of HF formation is in agreement with QMC calculations [22] for a finite-size Kondo cluster on a $2d$ square lattice and is caused by the crossover from a MIAM of the first kind to a MIAM of the second kind [4].

In the case of $N_f = 7$, the gap width in the spectral function of the central orbitals already agrees astonishing well with a full DMFT(NRG) calculation for a Kondo lattice with a Kondo coupling obtained from a Schrieffer-Wolff transformation of the corresponding SIAM for $N_f = 1$.

Using two techniques, (i) a supercell analysis for the uncorrelated limit and (ii) the extended Lieb-Mattis theorem for the strongly interacting and PH symmetric MIAM on a bipartite lattice, which originally were developed to make a statement on the nature of the ground state in a Kondo hole problem [24], we predicted the essential feature of the spectra at the Fermi energy of an orbital at an arbitrary site l: If the degeneracy of the ground state is enhanced by removing that orbital, the spectra needs to be fully gapped, $\rho_l(\omega = 0) = 0$, whereas it is finite if the degeneracy remains constant, $\rho_l(\omega = 0) > 0$. These predictions are in perfect agreement with our $1d$ NRG calculations and can be summarized as follows: (i) The spectra of the f orbitals at the edge of the impurity array are always metallic, independent of the strength of correlations. (ii) In the case of nearest-neighbor hopping between the c orbitals, the remaining spectra are fully gapped at $\omega = 0$ in the uncorrelated limit, according to the supercell analysis. (iii) In the strongly interacting limit, either all of the f orbitals acquire a finite spectra at $\omega = 0$ if the finite size c-f-orbital cluster is coupled to both of the sublattices of the remaining continuum or the $\omega = 0$ spectra oscillates as function of the sublattice index otherwise. Note that our numerical results demonstrate a rapid decrease of $\rho(\omega = 0)$ with increasing distance to the boundary of the f-orbital array such that a fully gapped bulk will be restored in the limit $N_f \to \infty$.

The finding of metallic surface states in the MIAM is in agreement with recent QMC calculations [22] for a finite-size Kondo cluster on a $2d$ square lattice, however, the oscillations of the spectra at $\omega = 0$ in the bulk have not been reported, even if the Kondo cluster only couples to one sublattice of the remaining continuum.

Since the experimental observation of metallic surface states in Kondo insulators triggered a lot of theoretical research with the focus on topological protection protected mechanisms caused by spin-orbit coupling, the finding of such states in the MIAM naturally raised the question, of how many additional uncorrelated c orbitals are needed in an extension of the conventional Kondo insulator description to obtain a metallic surface. Using the Lieb-Mattis theorem in combination with a mean-field calculation, we demonstrated that the removal of only the outermost f orbitals in a $2d$ Kondo insulator is sufficient to realize a metallic band that is exponentially localized at the boundary.

We studied the change in the site-dependent spectra upon introducing a Kondo hole in the center of a $N_f = 7$ cluster model. Shifting the on-site energy ϵ^h of the uncorrelated hole orbital from $\epsilon^h = 0$ to $\epsilon^h = \infty$, the model undergoes a Kosterlitz-Thouless-type QPT at a critical ϵ^h_c which is in accordance with the extended Lieb-Mattis theorem [24]. For $\epsilon^h \to \epsilon^h_c$, a Kondo resonance develops inside the gap of all f orbitals in the cluster, whose width gets exponentially suppressed at the QCP. In addition, a collective excitation is observed in the form of a sharp resonance that crosses

the Fermi energy already for $\epsilon^h < \epsilon_c^h$ and signals the reduction of charge carriers by one due to the removal of the hole orbital.

ACKNOWLEDGMENTS

The authors would like to thank Fakher Assaad for fruitful discussions.

[1] B. A. Jones and C. M. Varma, Study of Two Magnetic Impurities in a Fermi Gas, Phys. Rev. Lett. **58**, 843 (1987).

[2] K. Ingersent, B. A. Jones, and J. W. Wilkins, Study of the Two-Impurity, Two-Channel Kondo Hamiltonian, Phys. Rev. Lett. **69**, 2594 (1992).

[3] N. Grewe and F. Steglich, Heavy fermions, in *Handbook on the Physics and Chemistry of Rare Earths*, Vol. 14, edited by K. A. Gschneidner, Jr. and L. Eyring (North-Holland, Amsterdam, 1991), p. 343.

[4] F. Eickhoff and F. B. Anders, Strongly correlated multi-impurity models: The crossover from a single-impurity problem to lattice models, Phys. Rev. B **102**, 205132 (2020).

[5] M. B. Maple, M. C. de Andrade, J. Herrmann, Y. Dalichaouch, D. A. Gajewski, C. L. Seaman, R. Chau, R. Movshovich, M. C. Aronson, and R. Osborn, Non Fermi liquid ground states in strongly correlated f-electron materials, J. Low Temp. Phys. **99**, 223 (1995).

[6] N. Grewe, One particle excitation spectrum of the Kondo-lattice, Solid State Commun. **50**, 19 (1984).

[7] F. Steglich, J. Aarts, C. D. Bredl, W. Lieke, D. Meschede, W. Franz, and H. Schäfer, Superconductivity in the Presence of Strong Pauli Paramagnetism: $CeCu_2Si_2$, Phys. Rev. Lett. **43**, 1892 (1979).

[8] H. v. Löhneysen, A. Rosch, M. Vojta, and P. Wölfle, Fermi-liquid instabilities at magnetic quantum phase transitions, Rev. Mod. Phys. **79**, 1015 (2007).

[9] M. Kasaya, F. Iga, M. Takigawa, and T. Kasuya, Mixed valence properties of YbB_{12}, J. Magn. Magn. Mater. **47-48**, 429 (1985).

[10] T. Kasuya, Physical mechanism in Kondo insulator, J. Phys. Soc. Jpn. **65**, 2548 (1996).

[11] P. Hlawenka, K. Siemensmeyer, E. Weschke, A. Varykhalov, J. Sánchez-Barriga, N. Shitsevalova, A. Dukhnenko, V. Filipov, S. Gabáni, K. Flachbart, O. Rader, and E. Rienks, Samarium hexaboride is a trivial surface conductor, Nat. Commun. **9**, 517 (2018).

[12] D. Kim, J. Xia, and Z. Fisk, Topological surface state in the Kondo insulator samarium hexaboride, Nat. Mater. **13**, 466 (2014).

[13] W. K. Park, L. Sun, A. Noddings, D.-J. Kim, Z. Fisk, and L. H. Greene, Topological surface states interacting with bulk excitations in the Kondo insulator SmB_6 revealed via planar tunneling spectroscopy, Proc. Natl. Acad. Sci. **113**, 6599 (2016).

[14] V. N. Antonov, B. N. Harmon, and A. N. Yaresko, Electronic structure of mixed-valence semiconductors in the LSDA + U approximation. II. SmB_6 and YbB_{12}, Phys. Rev. B **66**, 165209 (2002).

[15] F. Lu, J. Z. Zhao, H. Weng, Z. Fang, and X. Dai, Correlated Topological Insulators with Mixed Valence, Phys. Rev. Lett. **110**, 096401 (2013).

[16] M. Z. Hasan and C. L. Kane, Colloquium: Topological insulators, Rev. Mod. Phys. **82**, 3045 (2010).

[17] M. Dzero, K. Sun, V. Galitski, and P. Coleman, Topological Kondo Insulators, Phys. Rev. Lett. **104**, 106408 (2010).

[18] V. Alexandrov, M. Dzero, and P. Coleman, Cubic Topological Kondo Insulators, Phys. Rev. Lett. **111**, 226403 (2013).

[19] J. Werner and F. F. Assaad, Interaction-driven transition between topological states in a Kondo insulator, Phys. Rev. B **88**, 035113 (2013).

[20] R. Peters, T. Yoshida, H. Sakakibara, and N. Kawakami, Coexistence of light and heavy surface states in a topological multiband Kondo insulator, Phys. Rev. B **93**, 235159 (2016).

[21] Y. Kuramoto, in *Theory of Heavy Fermions and Valence Fluctuations*, edited by T. Kasuya and T. Saso (Springer Verlag, Berlin, 1985), p. 152.

[22] M. Raczkowski and F. F. Assaad, Emergent Coherent Lattice Behavior in Kondo Nanosystems, Phys. Rev. Lett. **122**, 097203 (2019).

[23] S.-Q. Shen, Total spin and antiferromagnetic correlation in the Kondo model, Phys. Rev. B **53**, 14252 (1996).

[24] F. Eickhoff and F. B. Anders, Kondo holes in strongly correlated impurity arrays: RKKY-driven Kondo screening and hole-hole interactions, Phys. Rev. B **104**, 045115 (2021).

[25] K. G. Wilson, The renormalization group: Critical phenomena and the Kondo problem, Rev. Mod. Phys. **47**, 773 (1975).

[26] R. Bulla, T. A. Costi, and T. Pruschke, The numerical renormalization group method for quantum impurity systems, Rev. Mod. Phys. **80**, 395 (2008).

[27] A. Georges, G. Kotliar, W. Krauth, and M. J. Rozenberg, Dynamical mean-field theory of strongly correlated fermion systems and the limit of infinite dimensions, Rev. Mod. Phys. **68**, 13 (1996).

[28] G. Kotliar and D. Vollhardt, Strongly correlated materials: Insights from dynamical mean field theory, Phys. Today **57**(3), 53 (2004).

[29] P. Nozières, Impuretés magnétiques et effet Kondo, Ann. Phys. (Paris) **10**, 19 (1985).

[30] N. Grewe, On the competition between magnetic and Fermi liquid phases in Kondo lattices, Solid State Commun. **66**, 1053 (1988).

[31] R. Sollie and P. Schlottmann, A simple theory of the Kondo hole, J. Appl. Phys. **69**, 5478 (1991).

[32] R. Bulla, A. C. Hewson, and T. Pruschke, Numerical renormalization group calculations for the self-energy of the impurity Anderson model, J. Phys.: Condens. Matter **10**, 8365 (1998).

[33] T. Jabben, N. Grewe, and S. Schmitt, Spectral properties of the two-impurity Anderson model with varying distance and various interactions, Phys. Rev. B **85**, 045133 (2012).

[34] J. R. Schrieffer and P. A. Wolff, Relation between the Anderson and Kondo Hamiltonians, Phys. Rev. **149**, 491 (1966).

[35] R. Peters, T. Pruschke, and F. B. Anders, A numerical renormalization group approach to Green's functions for quantum impurity models, Phys. Rev. B **74**, 245114 (2006).

[36] A. Weichselbaum and J. von Delft, Sum-Rule Conserving Spectral Functions from the Numerical

Renormalization Group, Phys. Rev. Lett. **99**, 076402 (2007).

[37] F. B. Anders and A. Schiller, Time-Dependent Numerical Renormalization Group Approach to Non-Equilibrium Dynamics of Quantum Impurity Systems, Phys. Rev. Lett. **95**, 196801 (2005).

[38] F. B. Anders and A. Schiller, Spin precession and real-time dynamics in the Kondo model: Time-dependent numerical renormalization-group study, Phys. Rev. B **74**, 245113 (2006).

[39] F. Eickhoff, B. Lechtenberg, and F. B. Anders, Effective low-energy description of the two-impurity Anderson model: RKKY interaction and quantum criticality, Phys. Rev. B **98**, 115103 (2018).

[40] I. Affleck, A. W. W. Ludwig, and B. A. Jones, Conformal-field-theory approach to the two-impurity Kondo problem: Comparison with numerical renormalization-group results, Phys. Rev. B **52**, 9528 (1995).

[41] B. Lechtenberg, F. Eickhoff, and F. B. Anders, Realistic quantum critical point in one-dimensional two-impurity models, Phys. Rev. B **96**, 041109(R) (2017).

[42] T. Pruschke, R. Bulla, and M. Jarrell, Low-energy scale of the periodic Anderson model, Phys. Rev. B **61**, 12799 (2000).

[43] D. Withoff and E. Fradkin, Phase Transitions in Gapless Fermi Systems with Magnetic Impurities, Phys. Rev. Lett. **64**, 1835 (1990).

[44] K. Ingersent, Behavior of magnetic impurities in gapless Fermi systems, Phys. Rev. B **54**, 11936 (1996).

[45] L. Fritz and M. Vojta, Phase transitions in the pseudogap Anderson and Kondo models: Critical dimensions, renormalization group, and local-moment criticality, Phys. Rev. B **70**, 214427 (2004).

[46] C. C. Yu, Numerical renormalization-group study of a Kondo hole in a one-dimensional Kondo insulator, Phys. Rev. B **54**, 15917 (1996).

[47] I. Titvinidze, A. Schwabe, and M. Potthoff, Ferromagnetism of magnetic impurities coupled indirectly via conduction electrons: Insights from various theoretical approaches, Phys. Rev. B **90**, 045112 (2014).

[48] O. V. Yazyev and L. Helm, Defect-induced magnetism in graphene, Phys. Rev. B **75**, 125408 (2007).

[49] J. J. Palacios, J. Fernández-Rossier, and L. Brey, Vacancy-induced magnetism in graphene and graphene ribbons, Phys. Rev. B **77**, 195428 (2008).

[50] B. Uchoa, V. N. Kotov, N. M. R. Peres, and A. H. Castro Neto, Localized Magnetic States in Graphene, Phys. Rev. Lett. **101**, 026805 (2008).

[51] J.-J. Chen, H.-C. Wu, D.-P. Yu, and Z.-M. Liao, Magnetic moments in graphene with vacancies, Nanoscale **6**, 8814 (2014).

[52] Y. Jiang, P.-W. Lo, D. May, G. Li, G.-Y. Guo, F. B. Anders, T. Taniguchi, K. Watanabe, J. Mao, and E. Y. Andrei, Inducing Kondo screening of vacancy magnetic moments in graphene with gating and local curvature, Nat. Commun. **9**, 2349 (2018).

[53] D. May, P.-W. Lo, K. Deltenre, A. Henke, J. Mao, Y. Jiang, G. Li, E. Y. Andrei, G.-Y. Guo, and F. B. Anders, Modeling of the gate-controlled Kondo effect at carbon point defects in graphene, Phys. Rev. B **97**, 155419 (2018).

[54] N. C. Costa, M. V. Araújo, J. P. Lima, T. Paiva, R. R. dos Santos, and R. T. Scalettar, Compressible ferrimagnetism in the depleted periodic Anderson model, Phys. Rev. B **97**, 085123 (2018).

[55] Note that $U_{l_c} = 0$ in this case, contrary to Fig. 4. Therefore, the $\epsilon^h = 0$ spectra at different sites are not fully identical to those plotted in Fig. 4.

[56] T. Esat, B. Lechtenberg, T. Deilmann, ChristianWagner, P. Krüger, R. Temirov, M. Rohlfing, F. B. Anders, and F. S. Tautz, A chemically driven quantum phase transition in a two-molecule Kondo system, Nat. Phys. **12**, 867 (2016).